

Chapter 6. Wave Refraction, Breaking and Other Near-Shore Processes

Christopher C. Wackerman

General Dynamics - Advanced Information Systems, Ann Arbor, MI, USA

Pablo Clemente-Colón

Office of Research and Applications, NOAA/NESDIS, Camp Springs, MD, USA

6.1 Introduction

Near-shore water regions generate a rich range of surface signatures observable by a Synthetic Aperture Radar (SAR) sensor, mainly due to effects of spatially changing water depths that cause variations in the ocean surface roughness. In the open ocean (sometimes referred to as blue water), the water depth is large enough that it has little to no effect on the surface signatures, and is often ignored in theories and simulations of surface waves. However, in the near-shore region (often referred to as green water), depths are much smaller and rapidly changing, and surface waves can “feel” the bottom, causing changes in how the waves propagate and the wave shape and, eventually, causing the waves to break before reaching land. All of this generates a very dynamic environment in which changing surface waves cause changing currents throughout the near-shore water column. These currents, in turn, interact with currents from other sources (such as tidal flow or river outflow), which, in turn, affect the surface waves that pass through them, among other interactions. The interaction and feedback among all of these processes are extremely complex and, hence, very difficult to model. To date there are still unanswered questions about the physics of the near-shore region and how processes relate to each other. Even more difficult is to model SAR signatures of these processes by adding scattering theories for the various surface features along with the velocity effects important to SAR imaging theory. These complexities make the near-shore region an area of on-going research.

The near-shore processes can be divided into three main effects identifiable by SAR signatures: (1) spatially-variant surface wave fields (caused mainly by wave refraction); (2) surf zones where wave breaking occurs; and (3) strong, spatially-variant, surface current fields. In this chapter we will discuss the SAR signatures typically generated by each of these major effects, and show that for most near-shore regions, these effects can be identified separately and interpreted.

Because of its great utility in interpreting SAR signatures in near-shore regions, the two-scale Bragg scattering model for SAR ocean imaging (discussed in more detail in Chapters 2 and 4) is summarized briefly in Section 6.2. Section 6.3 subsequently discusses SAR signatures of the spatially-variant wave fields found in near-shore regions and what can be inferred from these patterns about water depth changes and surface currents. In Section 6.4 we discuss the breaking wave signatures found in the surf zone, how they are created, and what can be inferred from them. Section 6.5 discusses near-shore currents, how they are caused, and how they can be interpreted. Finally, we need to acknowledge that it is in the near-shore regions where most recreation and fishing activities occur, and thus these regions are abundant with man-made objects. Therefore, in Section 6.6, we show examples of SAR signatures of fishing vessels that are often observed in the imagery.

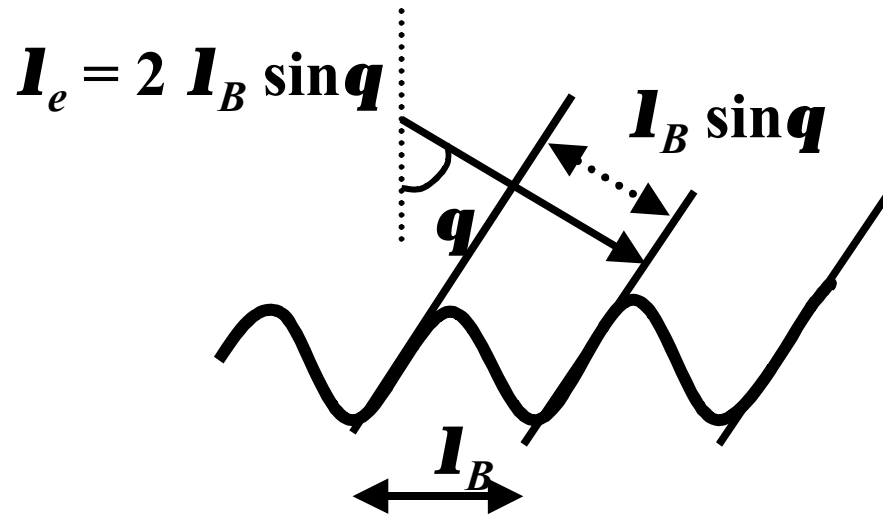


Figure 6.1. Illustration of Bragg scattering. The radar electromagnetic wavelength is λ_e , the wavelength of the ocean surface wave is λ_B , and the incident angle of the radar is θ . For the energy backscattered from the ocean wave peaks to be in phase (i.e., the wave is resonant with the radar radiation) the distance that the radiation travels between peaks ($\lambda_B \sin \theta$) must be equal to half the wavelength of the radiation. Thus, we must have $\lambda_e = 2\lambda_B \sin \theta$.

6.2 Summary of SAR Ocean Imaging

Because of its power in interpreting near-shore signatures, the simple two-scale Bragg scattering theory for SAR ocean imaging [Wright, 1968; Valenzuela, 1978; Plant, 1986; Romeiser *et al.*, 1997] is reviewed briefly in this section. Bragg scattering theory utilizes two ideas: (1) that the radar cross section observed by a SAR for a patch of ocean surface can be modeled strictly by the scattering from so-called Bragg waves; and (2) that the ocean surface can be considered to consist of two scales of waves: small-scale waves on the order of Bragg waves and large-scale waves on the order of three times the Bragg wave length or larger. The first idea is the Bragg scattering component, the second idea is the two-scale component.

Bragg scattering assumes that the radar cross section (and thus the brightness of the cross section in the SAR image) of a patch of ocean is determined strictly by the amplitude of the small-scale waves called Bragg waves (and in fact is proportional to this amplitude). Bragg waves are ocean surface waves which have wavelength equal to the projection of the SAR electromagnetic wavelength onto the local ocean surface and which are propagating either directly toward or away from the look direction of the sensor. This can be expressed by

$$l_B = \frac{l_e}{2 \sin q} \quad (1)$$

where λ_B is the wavelength of the Bragg wave, λ_e is the SAR electromagnetic radiation wavelength, and q is the local incident angle of the ocean surface (see Figure 6.1). The Bragg wave is the ocean wave that is resonant with the SAR electromagnetic wave in that all of the electromagnetic wavefronts scattering from different portions of the ocean wave come back to the sensor in phase (i.e., the backscattered radiation travels an integral number of wavelengths back to the sensor). Thus, the waves add constructively (see Figure 6.1 for an illustration) and cause a bright response in the SAR image that is considered the only contributor to the ocean surface radar cross section. Since most existing SAR sensors operate with electromagnetic

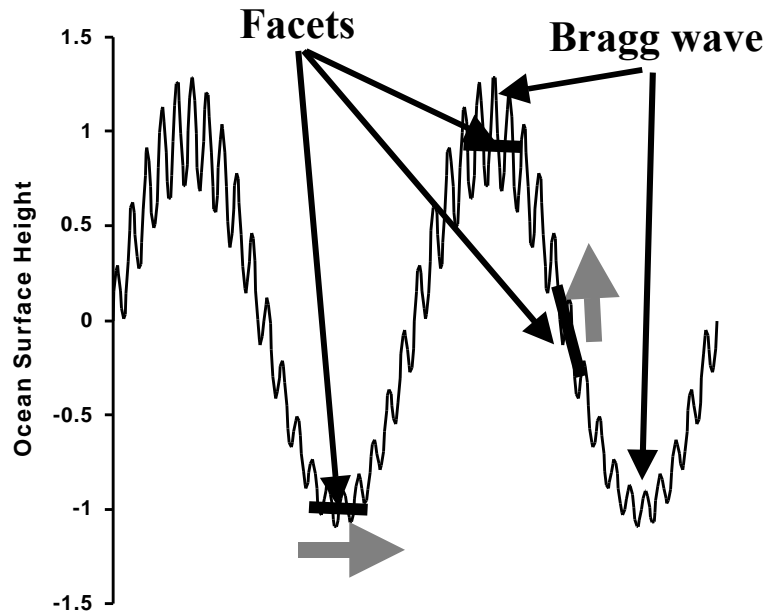


Figure 6.2. Example of the two-scale model where facets are shown as straight lines along the wave and the Bragg wave is shown as a smaller wavelength wave riding on the longer wavelength wave. The motion of two facets caused by the passage of the long wavelength wave is indicated with the large, gray, arrows.

wavelengths between 3 and 23 centimeters, their corresponding Bragg waves can be very small scale. Using the Bragg model, the radar cross section signature of any ocean feature can be calculated if we know how the Bragg wave amplitudes change as they interact with the feature. The feature will generate a bright signature if it causes an increase in the Bragg wave amplitude or a dark signature if it causes an amplitude decrease.

The ocean surface wave that is resonant with the SAR electromagnetic radiation (i.e., the Bragg wave) depends on the local slope of the ocean surface (that is the incident angle, θ , in Figure 6.1) since it depends on how the SAR electromagnetic radiation projects onto the surface. This means that the changes in ocean surface slope caused by the passage of large-scale waves are important for determining which ocean surface wave corresponds to the Bragg wave. The passage of large-scale waves also affects the motion of the Bragg wave scatterers since the Bragg waves interact with the orbital velocities of the large-scale waves. This motion has a very important effect in SAR imaging; radial motion shifts where the target is imaged, whereas azimuth motion smears the target signature (see Chapter 2 for more information on SAR motion effects). To handle both of these phenomena, we bring into the model the two-scale assumption. The two-scale model assumes that we can break the ocean surface into two scales; small-scale Bragg waves (wavelengths less than approximately 1 m) and large-scale surface waves (wavelengths greater than approximately 10 m). We then model the ocean surface as a series of flat plates. The flat plates have length scales on the order of a few Bragg wavelengths, and they are riding on the ocean surface. The surface height is determined by the sum of all the large-scale waves. Each plate is considered a flat surface consisting of Bragg waves; the amplitude of these waves determines the radar cross section of the plate. The slope of the plate is determined by the slope of the underlying large-scale waves at that location (the slope of the underlying waves is needed to determine the local angle of incidence and, thus, the wavelength of the ocean wave that corresponds to the Bragg wave). The motion of the plate is determined by the

instantaneous surface velocities of the underlying large-scale waves caused mainly by the orbital velocities of the large-scale waves.

The combination of Bragg scattering with the two-scale assumption is illustrated in Figure 6.2, which shows a one-dimensional cut through an idealized ocean surface consisting of a single large-scale wave and a single small-scale Bragg wave. The plates are illustrated with arrows indicating their motion as determined by the large-scale waves. The amplitude of the Bragg wave on each plate would determine the radar cross section of the plate.

The usefulness of this model for interpreting SAR signatures, particularly in the near-shore region, comes largely from its capability to break the problem into two pieces. First, we consider how the large-scale waves are being affected by the feature--in particular how their surface velocities are changing. Second we consider how the small-scale Bragg waves' amplitudes are changing. The former gives us the motion effect we will see in the SAR image, along with the changes in which surface wave will correspond to the Bragg wave. The latter gives us the expected changes in brightness of the feature.

The model summarized here is a simplified form of the more general model. For example, it is known that the large-scale surface velocities not only move the plates, but also affect the amplitudes of the Bragg wave riding on those plates, since the Bragg waves are also moving through the surface velocity field. This phenomenon is referred to as a hydrodynamic modulation of the Bragg waves, and a number of theories have been put forth to account for it [Alpers and Hasselmann, 1978; Alpers *et al.*, 1981; Plant, 1989; Plant, 1992; Romeiser *et al.*, 1994]. In addition, it is known that the small-scale waves also move and thus need to be accounted for in the SAR imaging theory [Hasselmann *et al.*, 1985; Bruening *et al.*, 1991]. This movement is often handled by assuming that the mean motion of the small-scale waves on a given plate is zero, but that the waves have some standard deviation of velocities that causes an azimuth smear in the image. Finally, a number of approaches have been developed to handle the intermediate-scale waves; waves with wavelengths between 1 m and 10 m which are ignored in the simple version [Lyzenga, 1998]. All of the above phenomena can be shown to be important when performing actual SAR image simulations, but are not necessarily useful in our more general interpretations.

6.3 Wave Refraction in the Near-Shore Region

The most significant environmental feature of the near-shore region is that water depths are shallow and change rapidly. The shallow depths mean that ocean surface waves can "feel" the bottom, which causes a change in how waves move, or propagate, along the surface, and a change in the shape of the wave as the depth gets shallower [Dean and Dalrymple, 1991]. A general rule of thumb is that a wave will start to be affected by water depth when the depth is less than or equal to half the wavelength. At this point, two main effects will start to occur. The first effect is that the wave will start to turn toward shore so that eventually the wave crests become parallel to the shoreline regardless of the angle at which they started in deeper water. This turning is referred to as wave refraction, and it occurs more rapidly (i.e., over shorter lengths) for regions where the depth is getting shallow faster than in regions where the depth change is gradual. Naturally, if the waves start in deep water with their crests parallel to shore, then wave refraction cannot be seen since there is no turning. The second effect is that the wavelength and amplitude of the waves change as depth gets shallower. In general, the wavelength will get smaller and the amplitudes larger as the wave shoals (i.e., moves into shore). Since these wavelength and amplitude effects are happening simultaneously, the wave is in fact

➔ SAR Look Direction

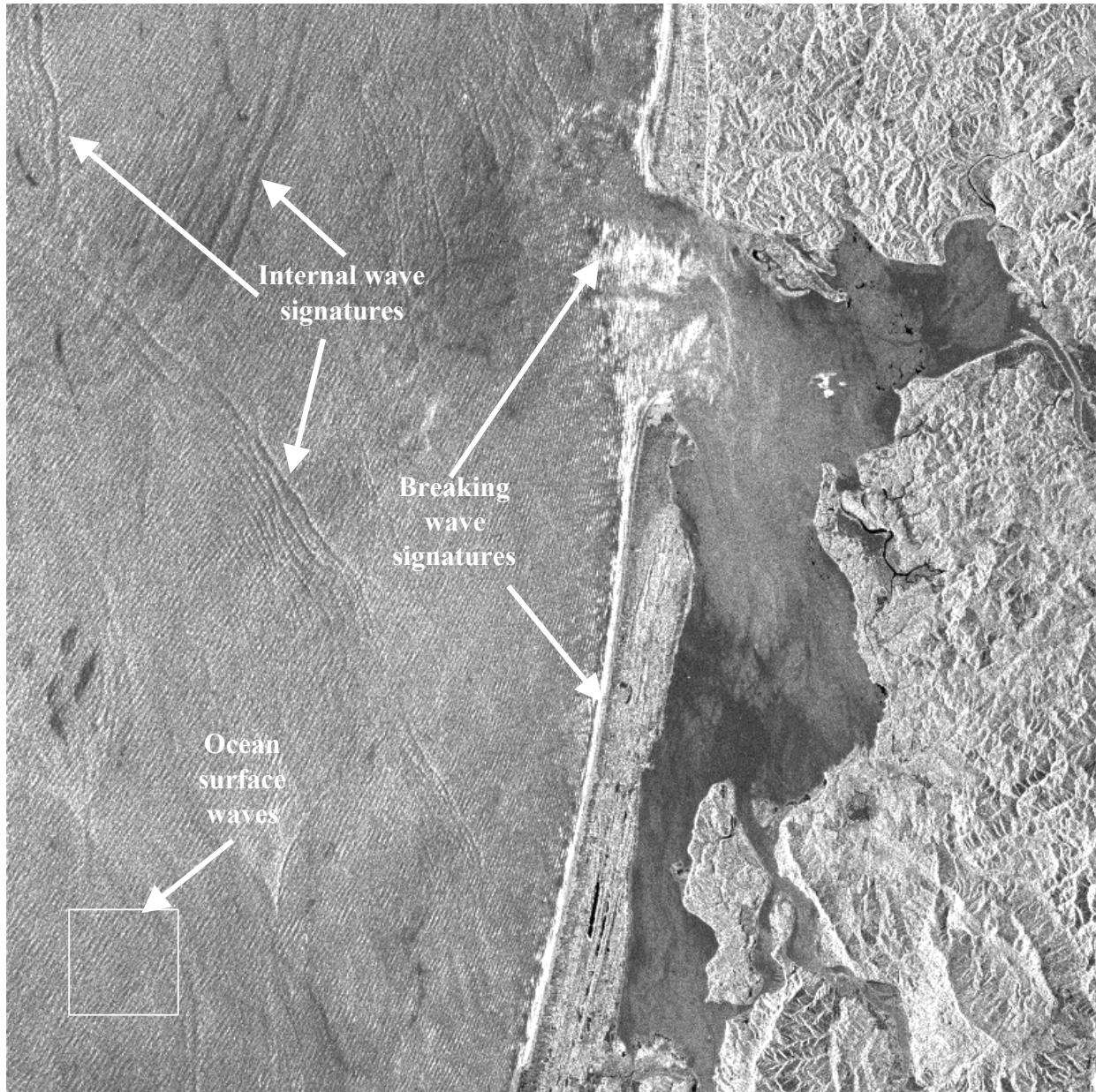
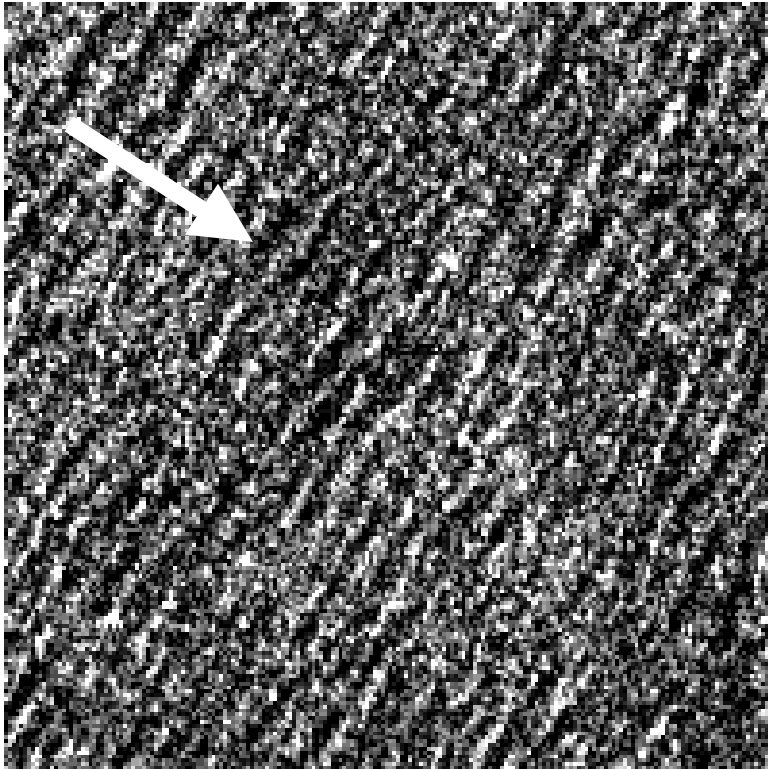


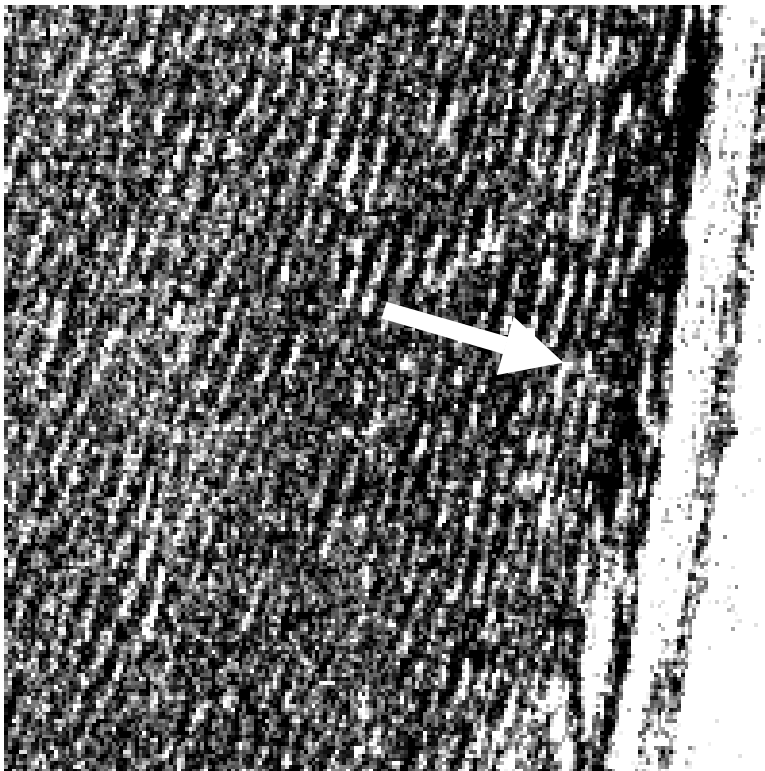
Figure 6.3. RADARSAT-1 (C-band, HH) SAR image of Willapa Bay, WA. An ocean surface wave pattern can be seen propagating generally from the upper left toward land. The refraction of the wave pattern as the waves shoal can be seen; Figure 6.4 provides a detailed view of the waves. The bright/dark linear features throughout the water regions are signatures from internal waves. The imaged area is 50 km x 50 km. ©CSA

getting steeper as it moves into shore, increasing the slope of its facets. Eventually, the wave gets so steep that it can no longer support the water and it breaks (breaking signatures are discussed in Section 6.4 below).

Taken together, these effects cause wave patterns to rotate and get shorter as the waves shoal (see Figures 6.3 and 6.4 for an illustration). The image in Figure 6.3 was collected by the



Deep water waves



Shallow water waves

Figure 6.4. Detailed view of a subset of the ocean waves in Figure 6.3 from a deep water region (top) and a shallow water region (bottom). The dominant wave direction is shown in each by a white arrow. Note the rotation of the wave pattern toward shore and the decrease in wavelength as the waves shoal. Each image covers an area 5 km x 5 km

Canadian RADARSAT-1 satellite SAR sensor that operates at C-band with HH polarization. The image covers 50 km on a side. Land can be seen on the right side of the image. The left side of the image represents deep water, and water depths decrease toward the land on the right. The image contains a number of near-shore features. The dark/bright wavy lines throughout the water are manifestations of internal waves (see Chapter 7). The brighter responses in the water along the shore and at the mouth of the bay result from breaking waves (see Section 6.4). An ocean surface wave pattern can be seen throughout the water, propagating in deeper water at approximately a 45 degree angle downward in the image, then rotating to make the wave crests parallel to shore in shallow water. One can also see that the wavelengths decrease from the deep water to the shallow water. To show this decrease more clearly, Figure 6.4 shows detailed views of the image in Figure 6.3 of a 5km x 5km patch of deep water (taken from the bottom of the image) and a 5km x 5km patch of shallow water. The wave propagation direction for each patch is indicated with an arrow. Figure 6.3 clearly shows the change in both direction and wavelength caused by wave refraction.

Wave refraction in SAR images can be used to estimate bathymetry; a classic process for studying ocean topography [Williams, 1947]. In Figure 6.3, one could determine the distance from shore that the wave system first begins to rotate toward shore and change its wavelength. This would represent the location at which the wave first is affected by the bottom. Using the general rule that a wave feels the bottom when the water depth is half the wavelength, one can estimate the wavelength of the deep water wave from the SAR image, and then estimate the water depth at the point when the wave first begins to refract. Although this is a coarse estimate, it can provide general information about depth changes.

Wave propagation models exist to predict wave refraction as a function of depth [Lui *et al.*, 1985]. By estimating the wave direction and wavelength throughout the image, one can get a better estimate of water depth by inverting these models; i.e., finding a depth map that generates the correct wave directions and wavelengths. Such an approach requires the assumption that the same wave train exists throughout the image, so that changes in wavelength are caused only by changes in depth. Automated algorithms that utilize this approach are currently being developed [Stockdon and Holman, 2000; Greidanus, 1997; Bell, 1999].

Finally, note in Figure 6.3 that the wave crests appear to get brighter as the waves shoal. This brightness increase is caused by the steepening of the long-scale waves, which causes a decrease in the local angle of incidence for the flat plate riding on the surface of the wave and, thus, an increase in the Bragg scattering (since the ocean surface wave that corresponds to the Bragg wave for these smaller angles of incidence has a larger amplitude).

6.4 Wave Breaking in the Surf Zone

Anyone who has stood on the beach and watched waves can attest to the violence of wave breaking. As waves approaching the shore, the water depth rapidly gets shallower causing the wave to increase its height and decrease its wavelength; both effects act together to increase the steepness of the wave. When the wave gets so steep that it can no longer support the water, the wave will break. Exactly when a wave breaks, and how it breaks, are matters of on-going research and no clear model exists. However, two prominently used approaches say wave breaking occurs when the downward acceleration of the water (caused by the passage of the steep wave) exceeds some percent of the gravitational constant, or that wave breaking occurs when the forward velocity of the water (again caused by the passage of the steepening wave) exceeds how fast the wave shape is moving (i.e., the phase velocity of the wave).

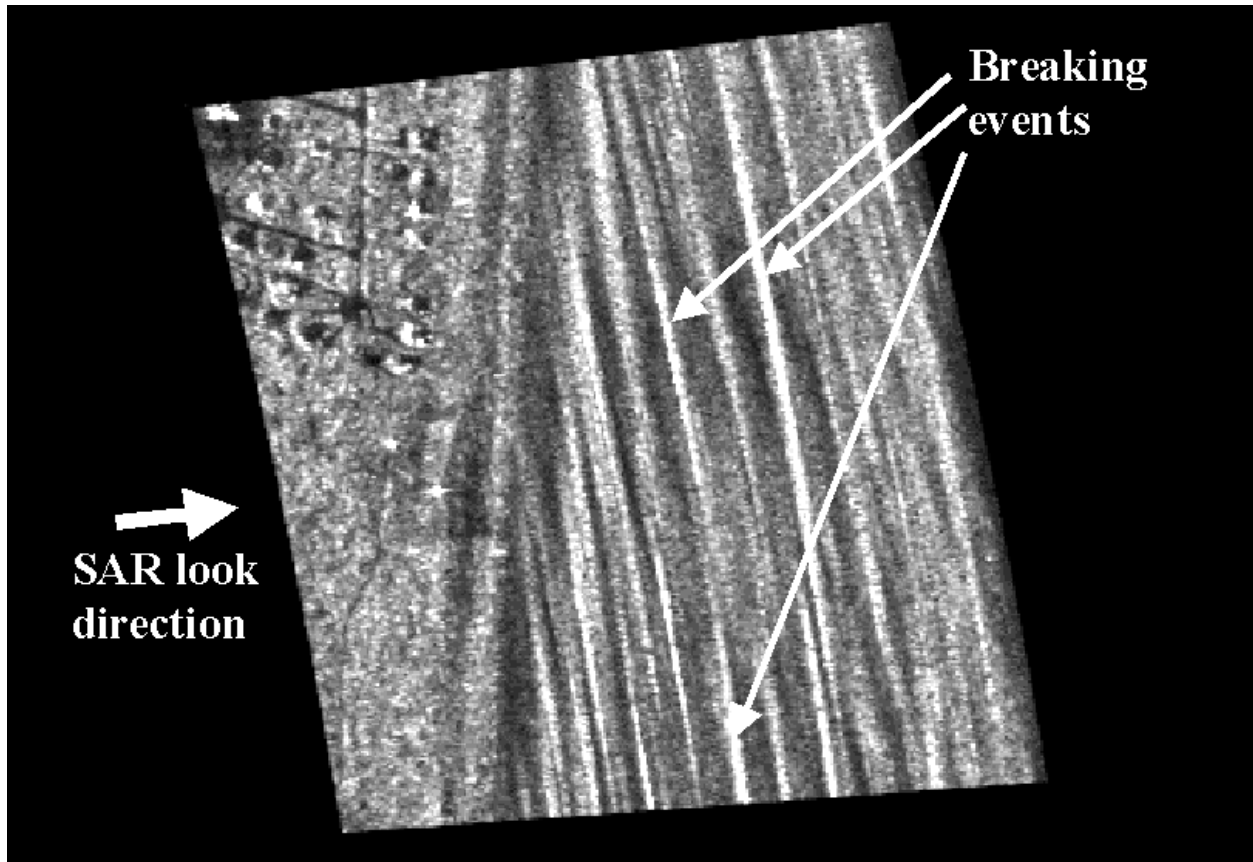


Figure 6.5. Fine resolution (2 m) airborne SAR image of breaking waves (X-band, HH). The bright smears are signatures of breaking events. Although the breaking events themselves are spatially small, the random motions in the breaking region cause the SAR image to be significantly smeared and shifted from the breaking location. Thus each smear in the image above represents one small-scale breaking event. Note that the smears are aligned in the azimuth direction (i.e., orthogonal to the SAR look direction) and that breaking is occurring throughout the water region of the image, indicating a high wave-state day. The imaged area is approximately 500 m x 500 m.

When a wave breaks, it creates a region of very turbulent, very rough, water [Peregrine, 1983; Battjes, 1988]. The increased roughness of the water produces an increase in the amplitude of the small-scale waves within the breaking regions, and thus implies a bright radar cross section for the breaking regions [Jessup *et al.*, 1991; Lee *et al.*, 1995; Chubb *et al.*, 1999; Ericson *et al.*, 1999]. In addition, the turbulence, or motion, of the water within the breaking region as well as the overall motion of the breaking region as it is being propagated along with the wave cause shifting and smearing effects in the SAR response. In particular, the speed at which the breaking region is propagating across the surface (usually some fraction, between 0.5 and 0.9, of the phase speed of the breaking waves) causes a shift in the azimuth direction of the SAR signatures by an amount, $(R/V) v_b$, where R is the range (i.e., distance) from the SAR to the region, V is the velocity of the SAR, and v_b is the radial velocity (the velocity along the line-of-sight direction back to the sensor) at which the breaking region is moving across the ocean surface. In addition, the turbulence in the breaking region causes random motion of the scatterers within the breaking region. This, in turn, causes a smearing of the SAR cross section where the width of the smear will be $(R/V)\sigma_b$ with σ_b being the standard deviation of velocities within the breaking region. Putting these pieces together, the SAR signatures of a breaking event will be a very bright smear, shifted in the azimuth direction some distance from the actual

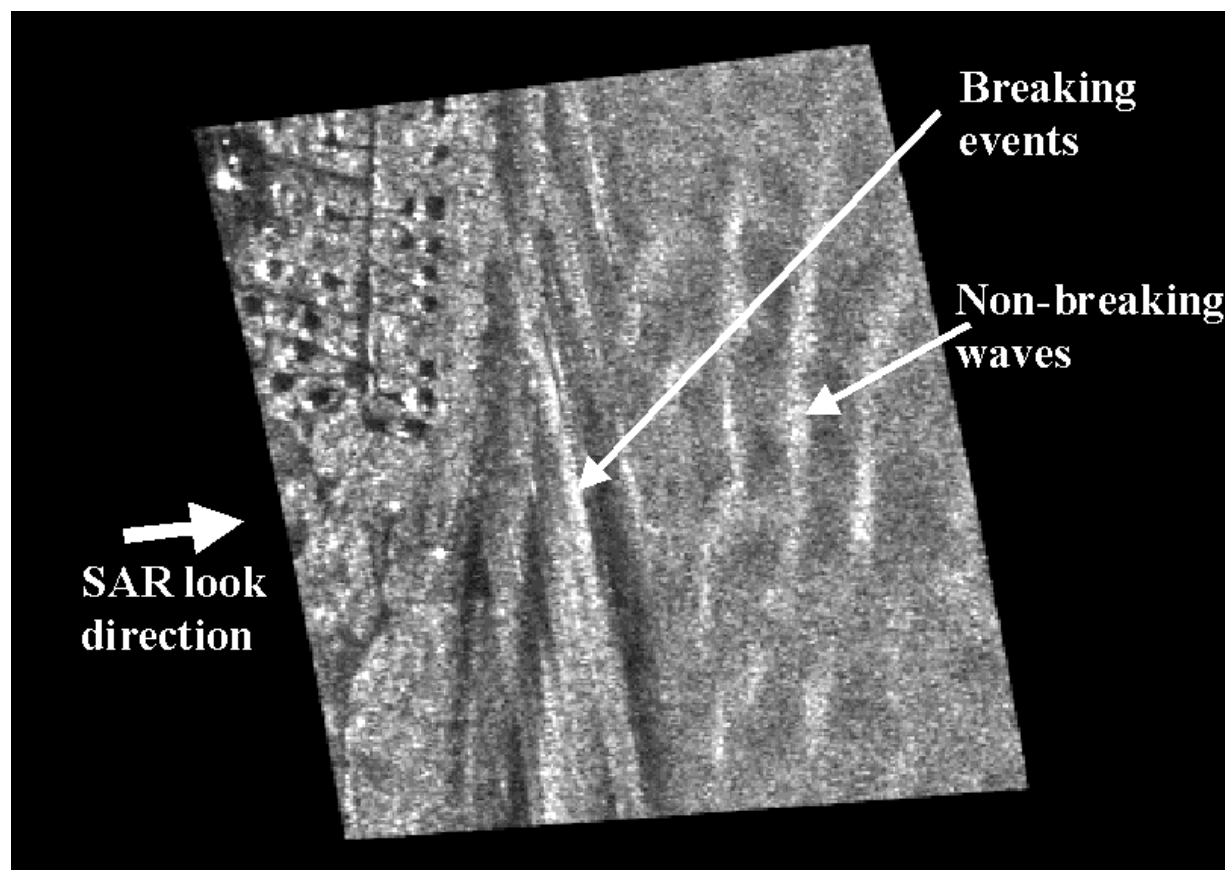


Figure 6.6. Fine resolution (2 m) airborne SAR (X-band, HH) image of breaking waves. This shows a much lower wave state than Figure 6.5. Note that the breaking is only occurring very near to shore and non-breaking waves can be seen in the water region. As in Figure 6.5, the imaged area is approximately 500 m x 500 m.

breaking region. For satellite-based SAR systems, such as RADARSAT-1 and ERS-1/2, the ratio (R/V) will be around 120. For breaking waves, values of v_b and σ_b will be around 1 m s^{-1} . This means that the breaking wave signatures could be shifted around 120 m from where the actual breaking is occurring, and the resulting smear could be around 120 m even if the breaking event is only occurring in a $1 \text{ m} \times 1 \text{ m}$ region. For an aircraft-based SAR, values of (R/V) are usually smaller, between 50 and 80. This means that the shifts and smears will be corresponding smaller; 50 m to 80 m.

A good example of this shifting and smearing is shown in Figure 6.5, an aircraft-based SAR (the Digital Collection System flown by Veridian Systems Division) image of the surf zone off the coast of Duck, North Carolina. This is a fine resolution SAR image (2 m sample spacing, X-band, HH polarization) and the streaks from the breaking events can clearly be distinguished on the right side of the image (some examples annotated in the image). The left-hand portion of the image shows land; note that houses on the shore can be distinguished. The look direction of the SAR sensor is also indicated in Figure 6.5, note that the smears from the breaking events are aligned orthogonal to the look direction (i.e., in the azimuth direction) even though the actual breaking waves must be aligned parallel to the shore (i.e., vertically in the image) because of wave refraction. As discussed above, each smear comes from a single breaking event which is probably no larger than a sample cell size (i.e., $2 \text{ m} \times 2 \text{ m}$), although in the image it looks like a large (i.e., 200 m long) breaking crest. However, the large size of the smear comes from the

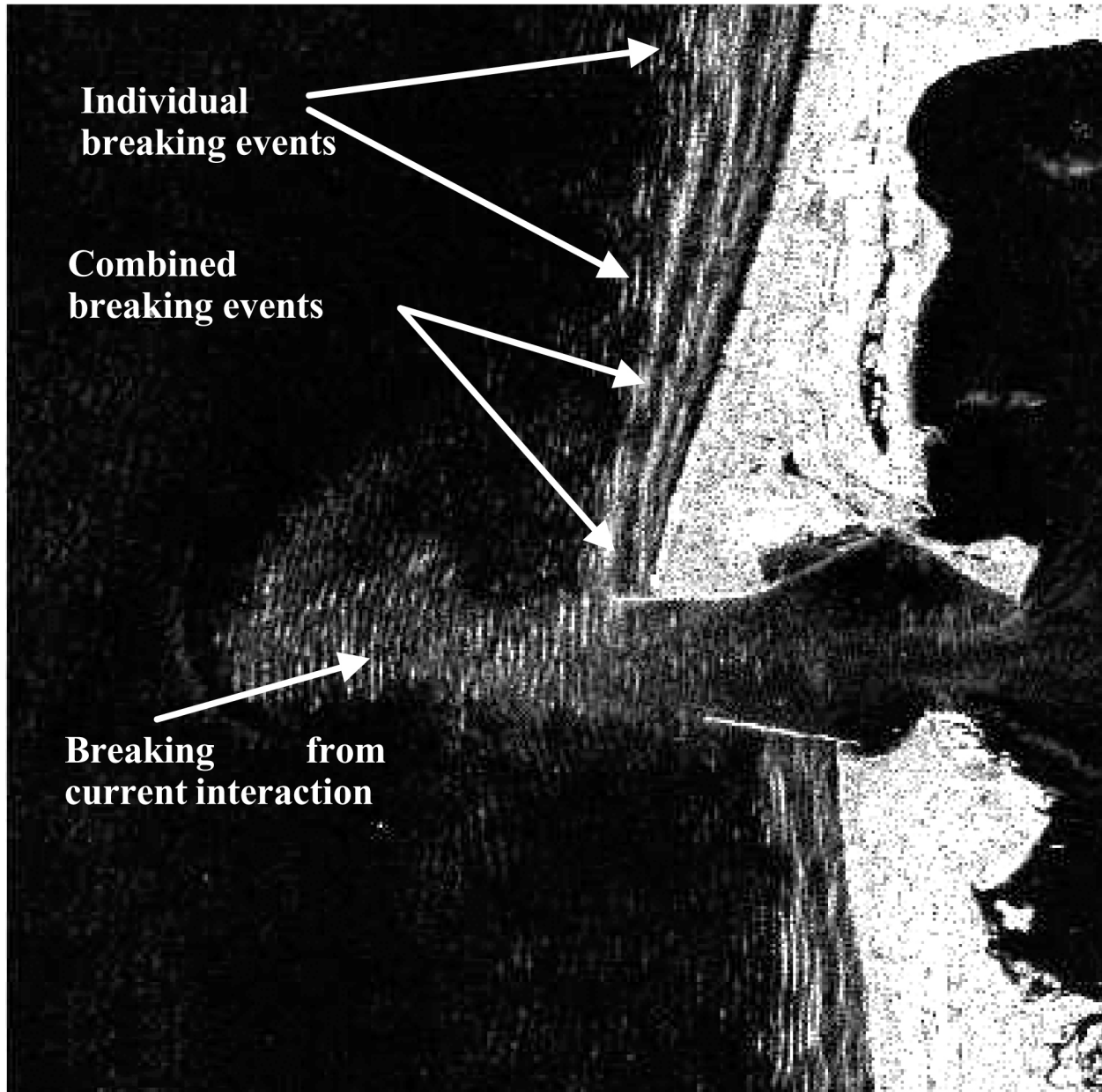


Figure 6.7. RADARSAT-1 (C-band, HH) SAR image of breaking waves off the coast of Washington (at Gray's Harbor). The image is approximately 25 km on a side. Note that farther from shore individual breaking events can be seen, but closer to shore they merge into a single bright band. Also note the breaking in the middle of the image that extends much farther out to sea than the breaking in the rest of the image. We conjecture that this is caused by the interaction of the waves with an outflowing current. The imaged area is 25 km x 25 km. ©CSA

SAR velocity effects discussed above and not the actual physical extent of the breaking event. This is why the smear is always in the azimuth direction, regardless of the actual physical orientation of the wave crests. In addition, note that the location of the breaking event is probably not where the smear appears, but rather is shifted in the azimuth direction as discussed above.

The image in Figure 6.5 was collected on a very high wave-state day, and breaking is occurring throughout the water region in the image. Figure 6.6 shows an example of the same

location, collected with the same airborne SAR system, for a much lower wave state. As annotated in the figure, the waves are only breaking near to shore. Non-breaking wave signatures can be seen in the right portion of the image. In contrast to the breaking events, non-breaking waves do not appear as narrow streaks, but rather bright regions aligned parallel to shore and not to the azimuth look direction.

It is interesting to note that if one knew the bathymetry of the region in Figures 6.5 and 6.6, then the wave state for that day could be estimated by noting where waves are breaking. A rule of thumb is that waves start to break when their heights are approximately 0.3 to 0.8 times the water depth [Mei, 1983]. For Figure 6.6, one can tell that the wave states must be rather small since the breaking is occurring close to shore, and thus at a shallow depth, and, therefore, with a smaller height at breaking. In contrast, Figure 6.5 shows breaking occurring all the way to the right edge of the image, showing that breaking is occurring at larger depths, and, therefore, higher wave amplitudes than in Figure 6.6.

Figures 6.5 and 6.6 are fine resolution images of breaking events. Satellite-based SAR systems, although they have larger smears, will have coarser resolutions and may not be able to distinguish individual breaking events since the events will be contained in a smaller number of image samples. Figure 6.7 shows an example of a RADARSAT-1 SAR image collected off the coast of Washington with 12.5 m sample spacing, where the breaking events can be seen as bright smears close to land. Note that individual smears (and thus breaking events) can be distinguished as the waves are just starting to break, but closer to shore the bright smears combine into a single bright region of multiple breaking events (which can be used to detect surf zone location and width). As with the earlier examples in this chapter, an estimate of the wave state (and, in particular, the height of the breaking wave) can be derived from noting where the breaking starts and comparing this to the local bathymetry. Figure 6.7 also shows an interesting example of wave breaking occurring from interaction with surface currents as opposed to breaking caused by changing water depth [Chawla and Kirby, 1998; Chawla and Kirby, 2002]. A water channel can be seen in the middle of Figure 6.7, having breaking signatures occurring much farther out to sea than either above or below the channel. If all the breaking in the image was being caused by shallow water depths, this would imply that there was a tongue of shallow depth in this middle region. However, channels tend to be dredged and thus deeper than the surrounding water, so we have hypothesized that the incoming ocean waves are hitting a surface current and breaking. Note that this implies that the current from the channel must be flowing out to sea at the time of the image collection since otherwise the incoming waves would not be breaking. This same phenomenon can be seen in Figure 6.3.

6.5 Near-Shore Currents

Near-shore regions tend to have strong currents that change rapidly over small spatial scales. Such rapid changes are caused by the many sources of currents in the near-shore region, including river outflow, rip currents (and undertow) caused by shoaling/breaking waves, and circulation effects caused by the continental shelf. What is important to interpreting SAR images of currents is the spatial change, or gradient, of the current [Lyzenga, 1991; Johannessen *et al.*, 1996; O'Donnell *et al.*, 2000]. See Chapter 8 for more details on SAR imaging of current fronts. SAR detects the effect that currents have on the amplitude of the Bragg waves (i.e., the two-scale model described above), and this effect is most pronounced when the Bragg waves interact with a sharp current change (i.e., a large current gradient). If a propagating Bragg wave suddenly moves into a current field that has a component in the direction that the wave is propagating, the



Figure 6.8. ERS-1 (C-band, VV) SAR image taken off the west coast of Norway on 3 October 1992. The bright/dark meandering linear features are signatures from strong current gradients that are perturbing the amplitude of the Bragg waves. The brightness of the signature (and whether it appears bright or dark) depends on the strength and orientation of the current gradient. The imaged area is 100 km x 300 km. ©ESA

wave length will increase, amplitude will decrease, and, thus, its radar cross section will decrease. In contrast, if the propagating Bragg wave enters a current field that has a component in the opposite direction from its propagation, this will decrease the wavelength, increase the amplitude, and increase the radar cross section. Note that once the Bragg wave has crossed the change in current, the local wind will cause the amplitude to relax to its previous state even though the mean current has changed. Thus the radar cross section in the two current fields will be the same even though the current is different. It is only when the Bragg wave experiences an abrupt change in current (i.e., it crosses a current gradient) that the wave amplitude is perturbed and, thus, the radar cross section is modulated.

Figure 6.8 shows an example of the effect of current change with an image collected by the ESA ERS-1 satellite-based SAR system (C-band, VV polarization). This image was collected off the west coast of Norway; land can be seen along the right side of the image. In these waters, the warm gulf currents interact with colder water moving south, thereby causing meandering current shears. Current shears are manifested in the SAR image as the curving dark/bright lines seen along the coast. The features are lines (as opposed to regions within the image) because they are only caused by the change in the Bragg wave amplitude when it first interacts with the new current field. The brightness of the feature is determined by the direction of the meandering current, as described above. This can be exploited to estimate the direction of the current from the SAR image and the strength of the current change by fitting the observed brightness to a model that predicts Bragg wave amplitude changes from the current gradient [Johanessen *et al.*, 1996].

Figure 6.9 shows a rather severe example of Bragg wave and current interactions in a RADARSAT-1 SAR image collected off of the east coast of the United States. The dominantly bright, curved lines throughout the ocean region represent near-shore currents interacting with the Bragg waves. Note that although most of the features are bright, there are some dark lines, and the orientation of the lines generally determines whether the line is bright or dark (lines sloping from upper left to lower right are bright, lines sloping from upper right to lower left are dark). The appearance of the lines is affected by orientation because, when the current gradient switches direction, the Bragg wave propagation direction with respect to the current direction changes, thus changing whether the Bragg waves are enhanced or suppressed. Figure 6.9 is a somewhat unique example in that the winds were most probably too light to significantly mix the upper layer of the ocean, thereby allowing these current patterns to be observed.

6.6 Man-Made Near-Shore Signatures

Most recreation and commercial fishing occurs in the near shore regions. Fishing operations (ships, nets, farms, floats, etc.) tend to be congregated in the near-shore region, and most recreational activities (swimming, boating, etc.) are performed in the near-shore region. Thus, signatures from these man-made events will often be present in SAR imagery. In general, man-made objects (or activities) in the water will have a much larger radar cross section than the water itself due to the fact that the water is generally flat (and thus generating radar cross section only through the two-scale model), whereas man-made objects tend to have edges and sides that act as very bright radar reflectors. Thus man-made signatures appear as bright dots in radar images; larger dots for ships, smaller dots (if visible at all) for floats, nets, and drifting bathers, for example. Figure 6.10 shows an example of a fishing fleet off the coast of Alaska collected with the RADARSAT-1 SAR at coarse resolution (100 m sample spacing). Note that the ships are quite evident as bright dots. Even though the ships may be smaller than the image sample

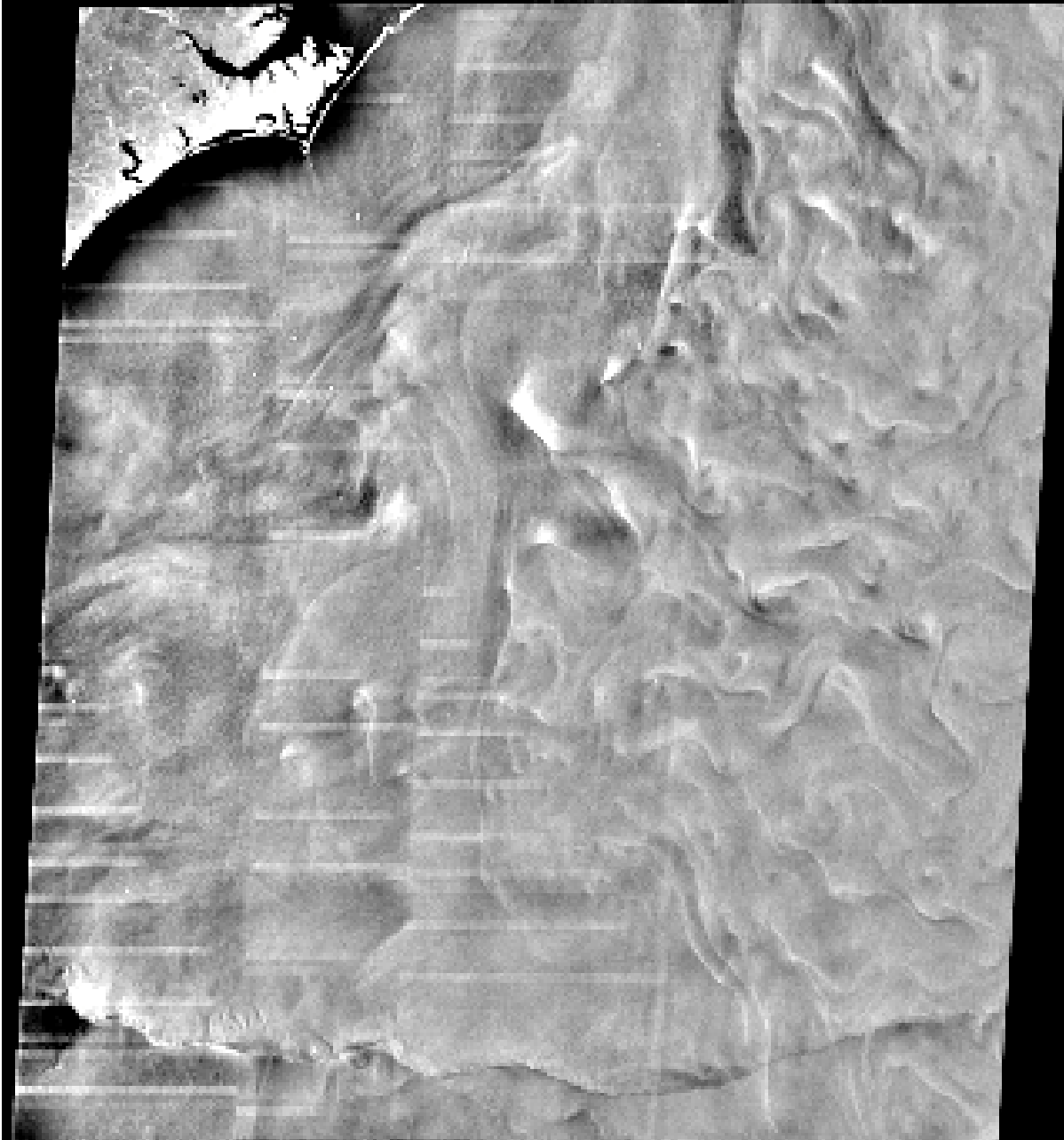


Figure 6.9. Example of current changes in the near-shore region. The bright/dark curvy lines represent current fronts in this RADARSAT-1 (C-band, HH) SAR image taken off the east coast of the United States. Note that the orientation of the lines generally determines its brightness (since orientation changes the direction that the Bragg waves are propagating with respect to the direction of the current gradient). The imaged area is 500 km x 500 km. ©CSA

size (100 m), they still are quite bright because they are the strongest radar cross section scatterer within the sample. Fishing ships will often be grouped close together as they are in the image. SAR imagery can be used to automatically locate and track ships such as these, providing a good means of monitoring fishing activities and fisheries [Wackerman *et al.*, 2001]. Note that the wave-like feature observed in the image moving through the water is actually a processing artifact, not an ocean surface wave.

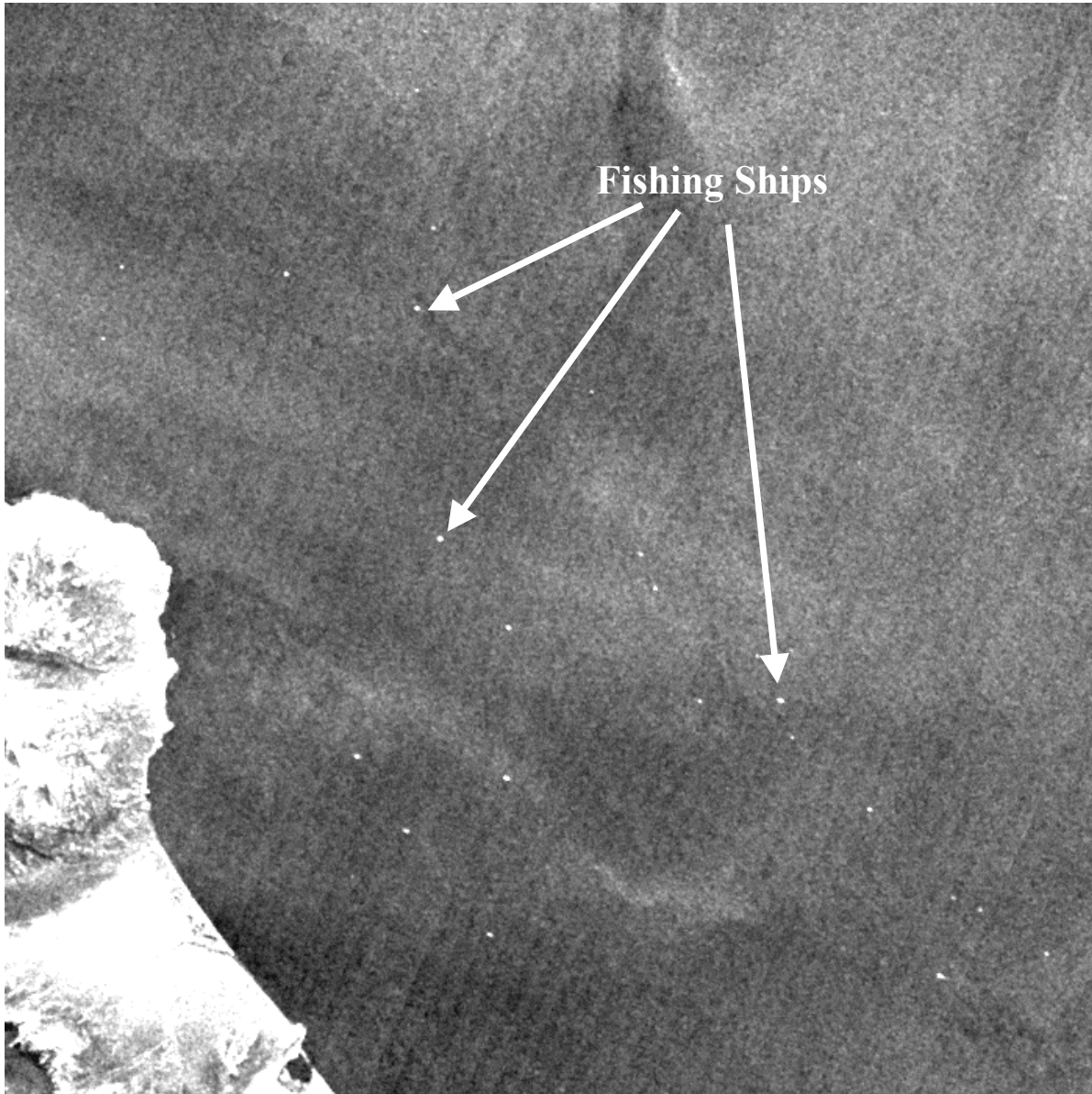


Figure 6.10. Fishing ships in Alaskan waters as seen by RADARSAT-1 (C-band, HH) SAR. As man-made objects, the ships appear as bright dots in the image. The imaged area is approximately 30 km x 30 km. ©CSA

6.7 Summary

Near-shore regions provide a rich array of oceanic features that can be imaged and interpreted with SAR data. Refracting waves can provide estimates of bathymetry or can locate regions of outflow. Breaking wave signatures indicate the location of the surf zone, identify bathymetry changes, and generate estimates of wave heights. Current fronts can be readily detected with SAR sensors, and their signatures in SAR imagery can be used to characterize the current gradient across the front. Finally, SAR sensors can easily detect large ships and fishing vessels, providing a means for monitoring fisheries and tracking recreational activities. In summary, near-shore regions provide a fertile ground for SAR imagery exploitation.

6.8 References

- Alpers, W., and K. Hasselmann, 1978: The two-frequency microwave technique for measuring ocean-wave spectra from an airplane or satellite. *Bound.-Layer Meteor.*, **13**, 215–230.
- , D. B. Ross, and C. L. Rufenach, 1981: On the detectability of ocean surface waves by real and synthetic aperture radar. *J. Geophys. Res.*, **86**, 6481–6498.
- Battjes, J. A., 1988: Surf-zone dynamics. *Annu. Rev. Fluid Mech.*, **20**, 257–293.
- Bell, P. S., 1999: Shallow water bathymetry derived from an analysis of X-band marine radar images of waves. *Coastal Eng.*, **37**, 513–527.
- Bruening, C., W. R. Alpers, and J. G. Schroter, 1991: On the focusing issue of synthetic aperture radar imaging of ocean waves. *IEEE Trans. Geosci. Remote Sens.*, **29**, 120–128.
- Chawla, A., and J. T. Kirby, 1998: Experimental study of breaking waves on a blocking current. *Proc. 26th Int. Conf. Coastal Engineering*, Copenhagen, Denmark, ASCE, 759–772.
- , and ——, 2002: Monochromatic and random wave breaking at blocking points. *J. Geophys. Res.*, **107**, 3067, doi:10.1029/2001JC001042.
- Chubb, S. R., A. L. Cooper, R. W. Jansen, R. A. Fusina, and J. S. Lee, 1999: Radar backscatter from breaking waves in gulf stream current convergence fronts. *IEEE Trans. Geosci. Remote Sens.*, **37**, 1951–1965.
- Dean, R. G., and R. A. Dalrymple, 1991: *Water Wave Mechanics for Engineers and Scientists*. Advanced Series on Ocean Engineering, Vol. 2, World Scientific, 353 pp.
- Ericson, E. A., D. R. Lyzenga, and D. T. Walker, 1999: Radar backscatter from stationary breaking waves. *J. Geophys. Res.*, **104**, 29 679–29 695.
- Greidanus, H., 1997: The use of radar for bathymetry in shallow seas. *Hydrogr. J.*, **86**, 13–18.
- Hasselmann, K., R. K. Raney, W. J. Plant, W. Alpers, R. A. Shuchman, D. R. Lyzenga, C. L. Rufenach, and M. J. Tucker, 1985: Theory of synthetic aperture radar ocean imaging: A MARSEN view. *J. Geophys. Res.*, **90**, 4659–4686.
- Jessup, A. T., W. K. Melville, and W. C. Keller, 1991: Breaking waves affecting microwave backscatter. 1. Detection and verification. *J. Geophys. Res.*, **96**, 20 547–20 559.
- Johannessen, J. A., R. A. Shuchman, G. Digranes, D. R. Lyzenga, C. Wackerman, O. M. Johannessen, and P. W. Vachon, 1996: Coastal ocean fronts and eddies images with ERS 1 synthetic aperture radar. *J. Geophys. Res.*, **101**, 6651–6667.
- Lee, P. H., and Coauthors, 1995: X band microwave backscatter from ocean waves. *J. Geophys. Res.*, **100**, 2591–2611.
- Lui, P. L. F., S. B. Yoon, and J. T. Kirby, 1985: Non-linear refraction-diffraction of waves in shallow water. *J. Fluid Mech.*, **153**, 185–201.
- Lyzenga, D.R., “Interaction of shore surface and electromagnetic waves with ocean fronts,” *J. Geophys. Res.*, **96**, 10765-10772, 1991.
- , 1991: Effects of intermediate-scale waves on radar signatures of ocean fronts and internal waves. *J. Geophys. Res.*, **103**, 18 759-18 768.
- Mei, C. C., 1983: *The Applied Dynamics of Ocean Surface Waves*. Wiley, 740 pp.
- O’Donnell, J. E. D., D. L. Miller, and C. C. Wackerman, 2000: RADARSAT SAR-derived ocean currents for operational maritime search and rescue planning. *Can. J. Remote Sens.*, **26**, 549–556.
- Peregrine, D. H., 1983: Breaking waves on beaches. *Amer. Rev. Fluid Mech.*, **15**, 149–178.
- Plant, W. J., 1986: A two-scale model of short wind-generated waves and scatterometry. *J. Geophys. Res.*, **91**, 10 735–10 749.
- , 1989: The modulation transfer function: concept and applications. *Radar Scattering From*

Wave Refraction, Breaking and Other Near-Shore Processes

- Modulated Wind Waves*, G. J. Komen and W. A. Oost, Eds., Kluwer Academic, 155–172.
- , 1992: Reconciliation of theories of synthetic aperture radar imagery of ocean waves. *J. Geophys. Res.*, **97**, 7493–7501.
- Romeiser, R., A. Schmidt, and W. Alpers, 1994: A three-scale composite surface model for the ocean wave-radar modulation transfer function. *J. Geophys. Res.*, **99**, 9785–9803.
- , W. Alpers, and V. Wismann, 1997: An improved composite surface model for the radar backscattering cross section of the ocean surface. Part 1: Theory of the model and optimization/validation by scatterometer data. *J. Geophys. Res.*, **102**, 25 237–25 250.
- Stockdon, H. F., and R. A. Holman, 2000: Estimation of wave phase speed and nearshore bathymetry from video imagery. *J. Geophys. Res.*, **105** (C9), 22 015–22 033.
- Valenzuela, G. R., 1978: Theories for the interaction of electromagnetic and oceanic waves—A review. *Bound.-Layer Meteor.*, **13**, 61–85.
- Wackerman, C. C., K. S. Friedman, W. G. Pichel, and P. Clemente-Colón, 2000: Automatic detection of ships in RADARSAT-1 SAR imagery. *Can. J. Remote Sens.*, **27**, 568–577.
- Williams, W. W., 1947: The determination of gradients on enemy-held beaches. *J. Roy. Geogr. Soc. London*, 109, 76-93
- Wright, J. W., 1968: A new model for sea clutter. *IEEE Trans. Antenna Propag.*, **16**, 17–223.